INTERACTION OF AN AIRCRAFT FUSELAGE BOUNDARY LAYER WITH A CONTRA-ROTATING TURBOFAN

Mouhamadou M. L. Diouf, Timea Lengyel-Kampmann, Rainer Schnell
German Aerospace Center DLR
Institute of Propulsion Technology, Linder Höhe, 51147 Köln, Germany

Abstract

Nowadays, global warming is one of the biggest issues for human being. A huge part of this warming is due to pollution from the transport industry and more particularly the aeronautical field. A lot of efforts are made in the turbofan engines design with the aim of improving the overall performance as well as respecting the environment (ACARE restrictions). To reduce fuel consumption, new aircraft concepts such as boundary layer ingesting (BLI) configurations are emerging [1]. BLI is a concept in which the engine ingests and reaccelerates the boundary layer from the aircraft fuselage in order to increase propulsive efficiency. It becomes then necessary to investigate the fan/BLI interactions and understand their detrimental influences on the fan performance. In this context, measurements are planned for 2019 at the Institute of Propulsion Technology of DLR in Cologne in which a generic and several real fuselage boundary layers are generated within a duct upstream of a contra rotating fan [2]. The aim of the present study is to provide results about the aerodynamic effects induced by BLI/fan interaction at given measurement locations [3]. This will be done by means of uRANS and Harmonic Balance based CFD computations involving different numerical setups and boundary conditions in order to quantify and isolate the different influential parameters. This is to understand the flow physics on the one hand as well as in order to prepare the cost intensive measurement campaign. In order to assess the dominant effects and most important influential parameters on the fan aerodynamic performance, relevant metrics such as the fan total pressure ratio, isentropic efficiency and the mass flow rate will be considered. In order to better understand the physical detailed interaction mechanisms, the results will also be analyzed based on local flow features as being observed in the CFD results.

ABBREVIATIONS

ACARE	Advisory Council for Aviation Research an innovation in Europe
a/c	Aircraft
BLI	Boundary Layer Ingestion
BPF	Blade Passing Frequency
CFD	Computational Fluid Dynamics
EO	Engine Order
GMC	General Mesh Connector
HB	Harmonic Balance
ISA	International Standard Atmosphere
PIV	Particle Imaging Velocimetry
RANS	Reynolds Average Navier-Stokes
RPM	Rounds per Minute
T/O	Take-Off
TRACE	Turbomachinery Research Aerodynamics Computational Environment

NOMENCLATURE

p_s	Static Pressure
p_t	Total Pressure
T_t	Total Temperature
v_{ax}	Axial Velocity
α_{tan}	Tangential velocity angle
σ	Inter Blade Phase Angle
f	Frequency
α, β	Flow Angles
T_u	Turbulence Intensity
l	Turbulent Length Scale
π_t	Total Pressure Ratio

1. INTRODUCTION

1.1. Background & Motivations

As the environmental impact of the nowadays aircraft engine is very high, the reduction of fuel consumption is of major concern. Several concept are continuously emerging, aimed at that goal. One of the most spoken concepts recently is Boundary Layer Ingestion (BLI). This concept was first suggested in the early 1930's. BLI deal specifically with the drag of the aircraft, trying to reduce it. In fact, in the case without boundary layer ingestion, the engine ingests a flow having the same velocity as the aircraft. The velocity is accelerated by the engine and has a higher value at the exit. This excess speed balances the speed deficit due to the drag of the aircraft. The main idea behind BLI is thus to ingest a part of the fuselage boundary layer inside the engines and reaccelerates it by embedding the nacelles to the fuselage, as show in fig 1. By doing so the kinetic energy of the jet, which is an unused energy for thrust production, is reduced leading to higher propulsive efficiency. This ingested boundary layer is seen by the engine as a total pressure

doi:10.25967/480125

distortion which will interact with the fan. Several studies has shown the positive effects of BLI in reducing fuel consumption[1] [4] [5] [6] [12].

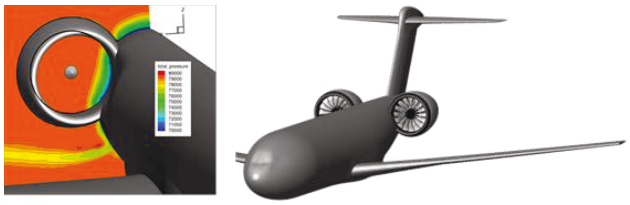

FIG 1. Boundary Layer Ingesting aircraft (DLR model)

However BLI has for sure some negative effects. It becomes then necessary to investigate the fan/BLI interactions and understand their detrimental influences on the fan performance. In this context, measurements are planned for 2019 at the Institute of Propulsion Technology of DLR in Cologne in which several distortions will be generated within a duct upstream of a contra-rotating fan.

1.2. Experimental setup overview

The DLR's experimental setup for BLI/fan investigation is shown in the figure 2 below. It has several measurement planes located along the axial direction and perpendicular to the flow direction.

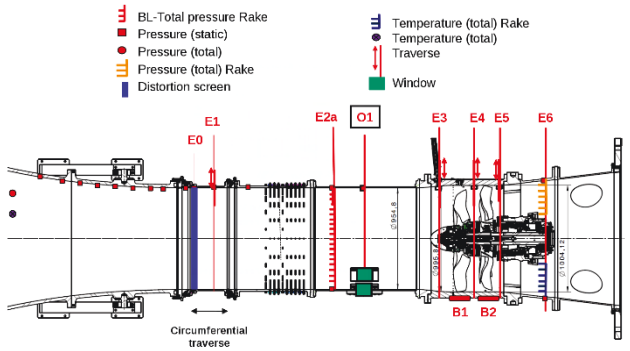

FIG 2. Experimental SETUP for BLI investigations

Different quantities are measured on each measuring location:

- **E0** is the plane where the total pressure distortion is generated using a distortion screen
- **E1** contains two hot-wire probes allowing to measure the three components of the flow velocity. It allows thus to test that there is not any turbulence (due to atmospheric conditions) affecting the measurements.
- **E2a** contains four total pressure rakes equidistantly distributed over the circumferential direction. The total pressure distribution in the entire plane can thus be measured.
- **E2b** contains four boundary layer rakes equidistantly distributed over the circumferential direction.
- **E3, E4, E5, E6** are respectively located in front of, between and behind the rotors. The first three mentioned contain each one Pt/Tt probe, two hot-wire probes, two PIV-Window and one PIV light beam. E6 contains 4 Pt/Tt rakes. They allow to measure all fan inflow and outflow condition and thus have access to the fan performances.

1.3. Scope of the paper

Since the experiments are very cost-intensive, a numerical setup is first performed in order to understand the flow physics for different operational parameters and prepare the measurement campaign. The present study aimed at answering the following questions:

- What effect does the BLI have on the fan aerodynamic performances ?
- What is the difference between a flat plate boundary layer and a real aircraft's fuselage boundary layer ?
- Which test cases (Distortion/RPM) are measurable with the given instruments as shown in Fig 2 ?

To doing so, the test cases, the numerical setup as well as the different settings will first be discussed in the next sections. In order to assess the dominant effects of the distortions and most important influential parameters on the fan aerodynamic performance, relevant metrics such as isentropic efficiency will be considered. In order to better understand the physical detailed interaction mechanisms of BLI/fan, the results will also be analyzed based on local flow features as being observed in the CFD results.

1.4. Test case overview

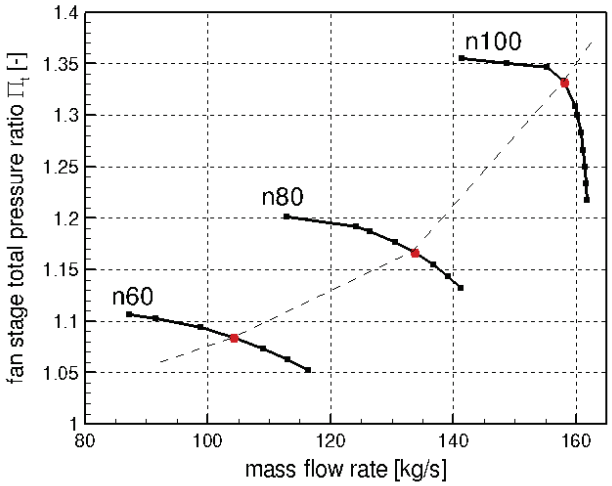

FIG 3. Fan performance characteristics of the selected RPM

Fig 3 shows the considered fan performance characteristics with the stage total pressure ratio variation versus the mass flow rate for 100%, 80% and 60% RPM. The three rotational speeds were

chosen from the Campbell diagram in such a way that the crossing between the engine orders (EO) and the torsion and the bending/flection modes are avoided. The points highlighted in red are the peak efficiency points for each rotational speed and are considered as reference points. For each RPM, the several distortions (see Fig 7) are computed with the same mass flow as the corresponding reference point.

2. NUMERICAL SETUP OVERVIEW

This study was conducted as part of the CRISP-II (Counter Rotating Integrated Shrouded Propfan) which aims at making a significant contribution to the economic and environmental performance of next-generation aircraft engines. The full geometry of the fan, designed and optimized by DLR (Köln) is composed by a spinner and two contra-rotating rotors. The front rotor (R1) contains 10 blades and the rear rotor (R2) has 12 blades.

2.1. Mesh

All measurement planes (except E6 plane) are in the calculation domain in order to be able to analyze and numerically visualize the quantities that will be measured. The mesh used for the inlet duct/fan model is presented in Fig 4 below. Both fan and inlet duct are meshed separately and assembled using the software GMC. The two rotors are meshed using an OCH topology, which means that the mesh is refined around the blade walls to handle strong gradients. The meshing of the inlet duct is mainly composed of radial bands with a stretch factor 1.1 at the tip and equally-spaced near the center. A “V-block” mesh is used near to r = 0. This mesh contains approximately three millions cells.

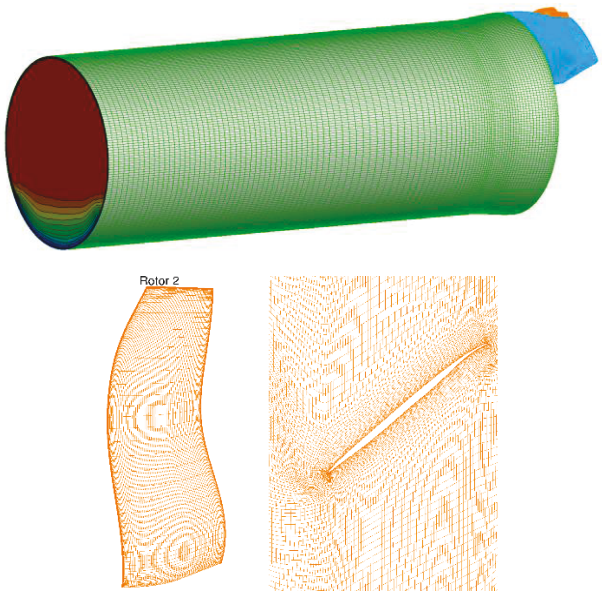

FIG 4. Mesh of the coupled inlet duct + fan

2.2. Boundary conditions

Fig 5 shows the different boundary conditions applied. An inlet condition is fixed in the computational domain entry where the total pressure distortion is imposed (in both experiment and simulation), as well as values of total temperature and flow angles. An outlet condition is used at the exit with a given back pressure value (static pressure); the radial equilibrium is located at midspan. A mixing plane interface condition is fixed at the front rotor outlet and the rear rotor inlet. It consists on an average in the circumferential direction on both the rotor outlet and the stator inlet. A moving condition is imposed on the two rotors. Finally, a viscous wall boundary condition is used in solid regions.

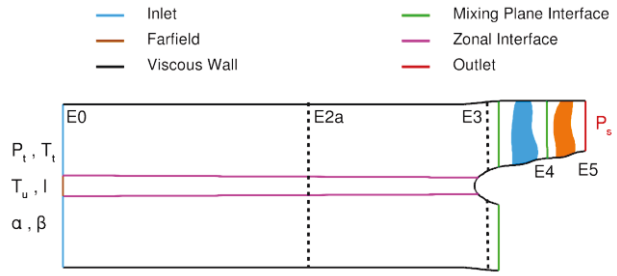

FIG 5. Boundary conditions applied

2.3. The Harmonic Balance Method

The Harmonic balance technique is a method used in general to simulate the unsteady interaction between Rotor/Stator of a turbomachinery component. It is a Fourier-based method applied to the frequency domain in order to solve semi discrete form of the Navier-Stokes equations given below:

$$V\frac{\partial q}{\partial t} + R(q) = 0 \quad (1)$$

where q is the vector of conservative variables and R(q) the residual vector from spatial discretization. The Harmonic Balance Method relies on three main hypothesis[7]:

- **q** is temporally periodic, which make use of Fourier transform.
- **the energy** is concentrated on a finite number of Harmonics N.
- **the turbulence** is fully modeled.

This technique is based on the concept of so-called harmonic sets. A harmonic set is defined by a base frequency f, a base interblade phase angle σ and a set of harmonic indexes $k_1, \dots, k_n$. A previous study has shown that eight harmonics are sufficient to capture the energy from the downstream disturbances (convective effects) while four is enough for the upstream ones (potential effects)[8]. It has also shown the ability of the harmonic balance to handle mixing plane interfaces.

The HB method in TRACE is formulated in the frequency domain. For each harmonic set, it solves :

(2) $iw\widehat{q_{w,\sigma}} + \hat{R}(q)_{w,\sigma} = 0$

Table 1 summarizes the harmonic sets used in this work.

TAB 1. Harmonic sets of each blade row.

Row	(f,σ)	
Inlet Duct (D)	$(BPF_{R1-D}, 0°)$ $(2BPF_{R1-D}, 0°)$ $(3BPF_{R1-D}, 0°)$ $(4BPF_{R1-D}, 0°)$	
Rotor 1 (R1)	$(BPF_{D-R1}, -36°)$ $(2BPF_{D-R1}, -72°)$ $(3BPF_{D-R1}, -108°)$ $(4BPF_{D-R1}, -144°)$ $(5BPF_{D-R1}, 180°)$ $(6BPF_{D-R1}, 144°)$ $(7BPF_{D-R1}, 108°)$ $(8BPF_{D-R1}, 72°)$	$(BPF_{R2-R1}, -72°)$ $(2BPF_{R2-R1}, -144°)$ $(3BPF_{R2-R1}, 144°)$ $(4BPF_{R2-R1}, 72°)$
Rotor 2 (R2)	$(BPF_{D-R2}, 30°)$ $(2BPF_{D-R2}, 60°)$ $(3BPF_{D-R2}, 90°)$ $(4BPF_{D-R2}, 120°)$ $(5BPF_{D-R2}, 150°)$ $(6BPF_{D-R2}, 180°)$ $(7BPF_{D-R2}, -150°)$ $(8BPF_{D-R2}, -120°)$	$(BPF_{R1-R2}, -60°)$ $(2BPF_{R1-R2}, -120°)$ $(3BPF_{R1-R2}, 180°)$ $(4BPF_{R1-R2}, 120°)$ $(5BPF_{R1-R2}, 60°)$ $(6BPF_{R1-R2}, 0°)$ $(7BPF_{R1-R2}, -60°)$ $(8BPF_{R1-R2}, -120°)$

2.4. Presentation of the inlet distortions

In order to better understand the complex flow physics behind fan/BLI interactions, it has been considered three different nacelles, having the same diameter and differently embedded to the fuselage. The embedment level (EG) is defined by the ratio between the submerged diameter in the fuselage and the engine diameter (as shown in figure 6 and Eq 3).

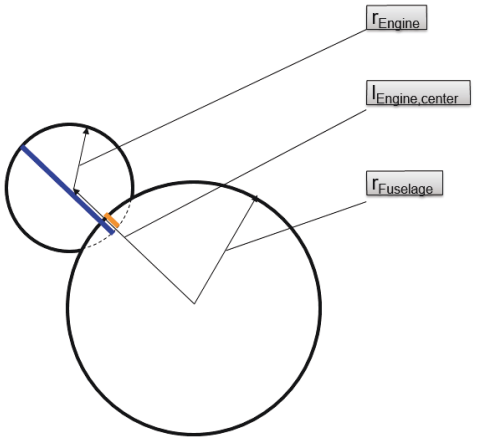

FIG 6. Sketch of an engine embedded to the fuselage

(3) $EG = \frac{r_{Engine} + r_{Fuselage} - l_{Engine,center}}{2.r_{Engine}}$

Fig 7 shows the inlet stagnation pressure distortions considered. It contains a generic boundary layer (vertically stratified distribution model of an ingested boundary layer of an airplane fuselage) and five real boundary layer (extracted upstream of the fan from the setup shown in fig 1 and fig 6, resulting from full aircraft CFD provided by the DLR's Institute of Aerodynamics and Flow Technology).

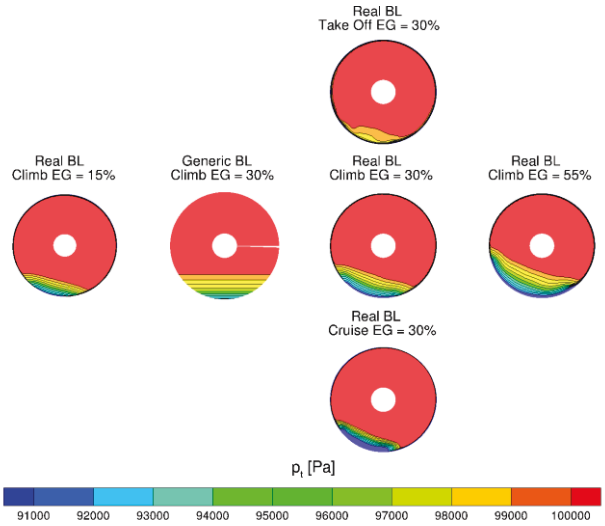

FIG 7. Total pressure distortions considered

Each represents disturbance for different embedded nacelle and flight conditions. The different inlet distortions are generated within a duct upstream of the contra-rotating fan and have the form of a turbulent boundary layer. The 30% embedded nacelle is the reference. From that configuration, the take-off ($Ma = 0.2$), climb ($Ma = 0.5$) and cruise ($Ma = 0.78$) disturbances have been determined. Then a lower embedded (15%) and a higher one (55%) are considered for the climb condition. The total pressure values have been reduced to ISA sea level conditions for easy comparison between the different distortions. Due to aeroelastic stability limits, the cruise distortion has not been simulated for this study.

3. FAN/BLI INTERACTION ANALYSIS

3.1. Flow physics

In order to understand the flow physics behind total pressure distortion, let's first consider the simplified approach proposed by Longley[9]. It has been considered two streams of different total pressure at the compressor intake. As the viscous forces were neglected, it has been demonstrated that the total pressure distortion is convected from far upstream to the compressor face, as shown in fig 8.

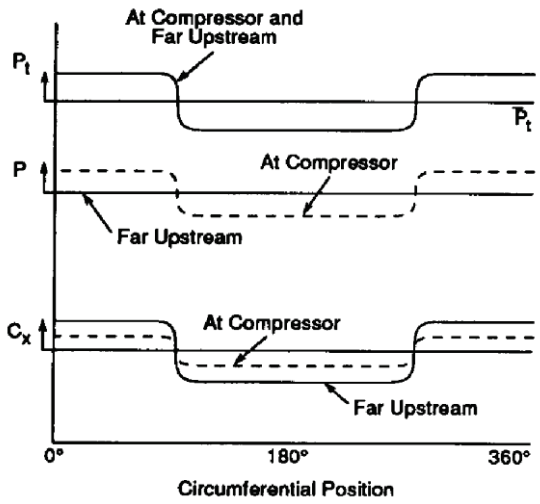

FIG 8. Total pressure, static pressure and axial velocity distortions at far upstream and at compressor[9]

Since the axial velocity at the compressor is non-uniform, there is a higher flow incidence near the distorted tip region, where the axial velocity values are lower. At far upstream, the static pressure is constant over the circumference while it is distorted at the compressor. This is due to a circumferential flow redistribution caused by the interaction between the distortion and the compressor. In fact, there is a not-equal fan pressure rise between the clean and the distorted sectors, leading to local operating points over the circumference.

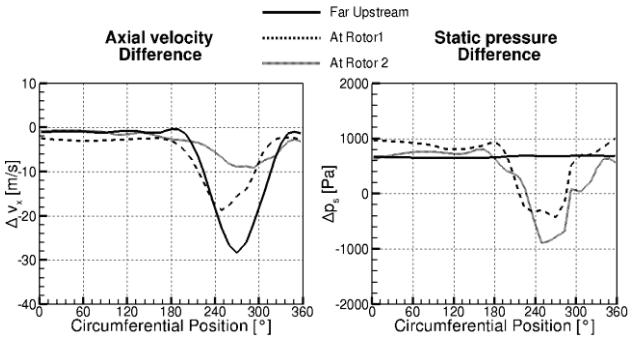

FIG 9. Axial velocity and static pressure distortions at far upstream ($\sim E0$), at rotor 1 ($\sim E3$) and at rotor 2 ($\sim E4$) (Generic BLI, n/n0=80%).

Fig 9 shows the axial velocity and static pressure distribution over the circumference at far upstream, at rotor 1 and at rotor 2 for the generic boundary layer computed at 80% RPM. On Longley's approach, the variations are creneau-shaped because it considered only two streams with different total pressures. The distortions considered in this study have several continuous levels of total pressure; the circumferential distributions of the flow variables are still very similar to the Longley approach. There is however a deflection of the distortion in the direction of rotation of rotor 1 and rotor 2. The axial velocity difference is almost constant behind the rear rotor. This shows the positive effects of the fan on attenuating the distortion.

To illustrate the previous observations, the axial velocity contours are depicted in fig 10 below at different locations upstream, in between and downstream of the fan. The inlet total pressure distortion appears as a decreased axial velocity levels at far upstream, which is convected from E0 to E3, where the diffusion from the spinner is also noticeable. The distortion is then redistributed in the circumferential direction and attenuated on the passage of each rotor.

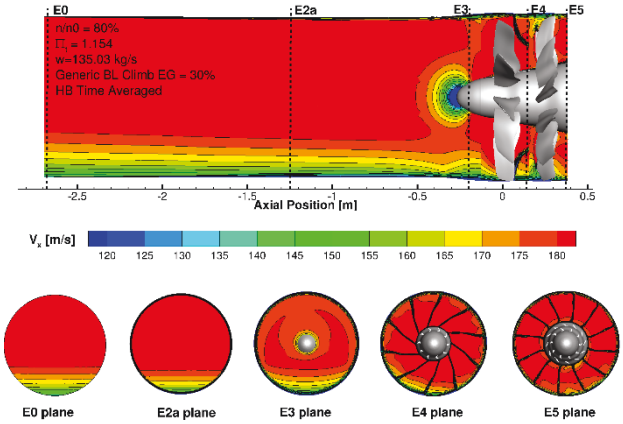

FIG 10. Axial velocity contours at different axial positions

Fig 11 shows the tangential velocity angle contours at difference axial positions. It can be seen that upstream of the fan (E3 plane) there is two zones of positive (co-swirl) and negative (counter-swirl) distortions, due to the local operating conditions seen by the fan. Downstream of the front rotor, the tangential velocity angle values are very high, which means that there is high energy loss (as swirl is not used to produce thrust); this energy is then retrieved by the rear rotor. This highlights the positive effects of using a counter-rotating turbofan.

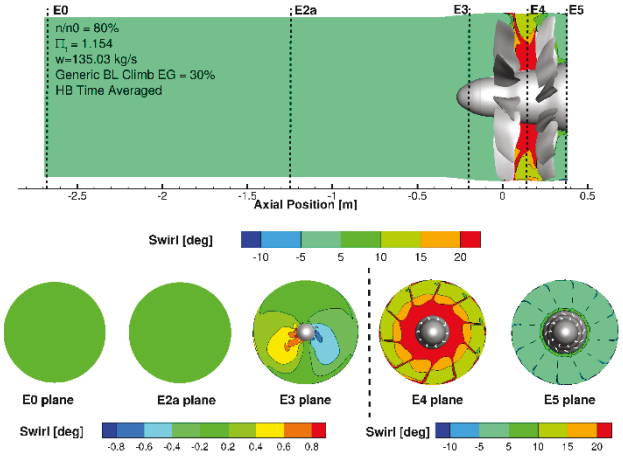

FIG 11. Tangential velocity angle contours at different axial positions

3.2. Difference between generic and real BLI

As shown in fig 6, two main types of distortions have been studied: a generic BLI which models a boundary layer over a flat plate and a real BLI which is a boundary layer from a real aircraft fuselage. Theoretically, an a/c fuselage boundary layer is much complex than a flat plate one since the 3D effects are not taken into account with the flat plate boundary layer. In fact, there are additional pressure gradients in the circumferential direction for the a/c fuselage boundary layer due to the shape of its geometry. This section is aimed at comparing to fan local operating points of each type of distortion.

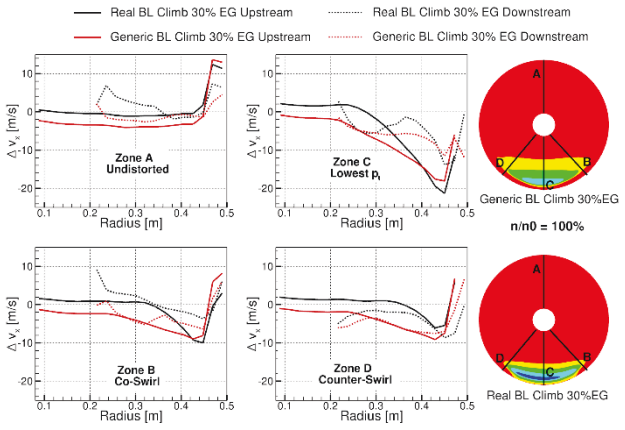

FIG 12. Comparison Generic vs Real BLI

Fig 12 shows for each distortion, the radial distributions of axial velocity difference (BLI/clean) at four circumferential positions (A, B, C, D) upstream (E3) and downstream (E5) of the fan. The four positions represents the main local operating conditions featured by BLI/fan interactions. It can be seen that the generic and the real boundary layer have a similar radial distribution for each circumferential position, whether it is upstream or downstream of the fan. The overall values for the generic boundary layer are however lower than the real boundary layer. This means that for the same embedded engine and operating point, the real a/c fuselage boundary layer has stronger effects on the fan than a flat plate boundary layer.

3.3. Effects of the different distortions (levels and flight conditions)

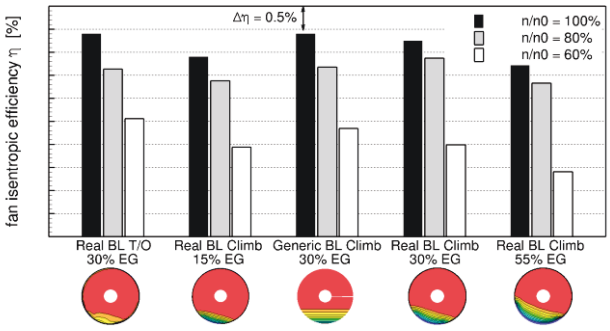

FIG 13. Fan isentropic efficiency vs the distortions

Fig 13 shows the average fan isentropic efficiency for each distortion and rotational speed. Bar chart has been plotted since there is a small difference between the disturbances in the performance map. The distortions effects are similar for each RPM. The take-off, which is the smallest distortion, has the highest efficiency, while the 55% embedded climb distortion has the lowest. It can also be seen that, for each distortion, the isentropic efficiency is as low as the rotational speed decreases.

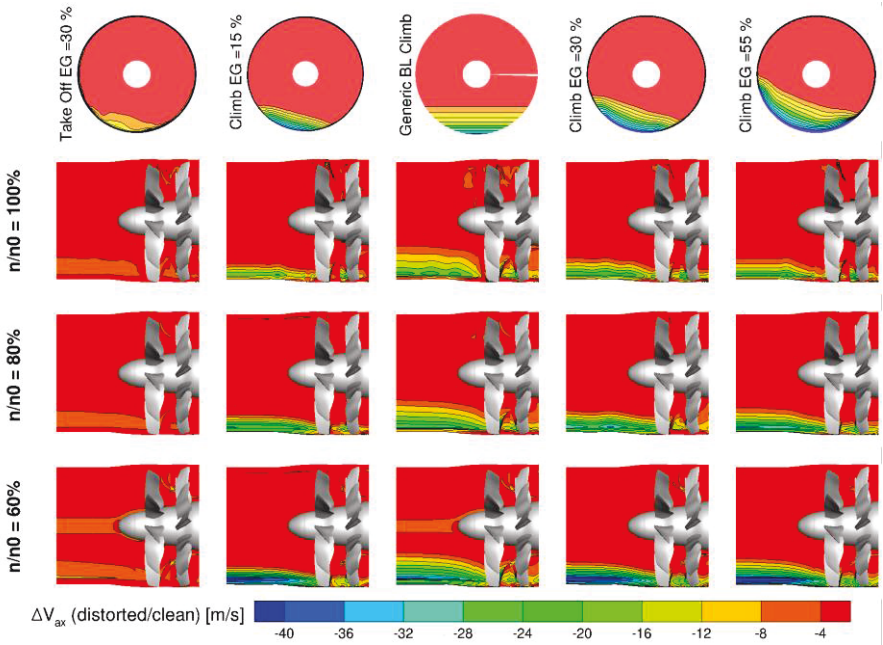

FIG 14. Axial velocity difference contours for several computed distortions and rotational speed

The instantaneous axial velocity difference contours is depicted in fig 14 for all couple (distortion/RPM). An axial view of the fan is shown, as the PIV measurements will the made in that plane. It is noticeable that for a given disturbance, the distortions effects are stronger at lower rotational speed. This is in agreement with drop of isentropic efficiency for lower rotational speed noticed earlier. For the same flight condition (ie Climb), the distortion effects are also stronger for deeper embedded engines. For a given rotational speed, the take-off has the lowest distortion effects.

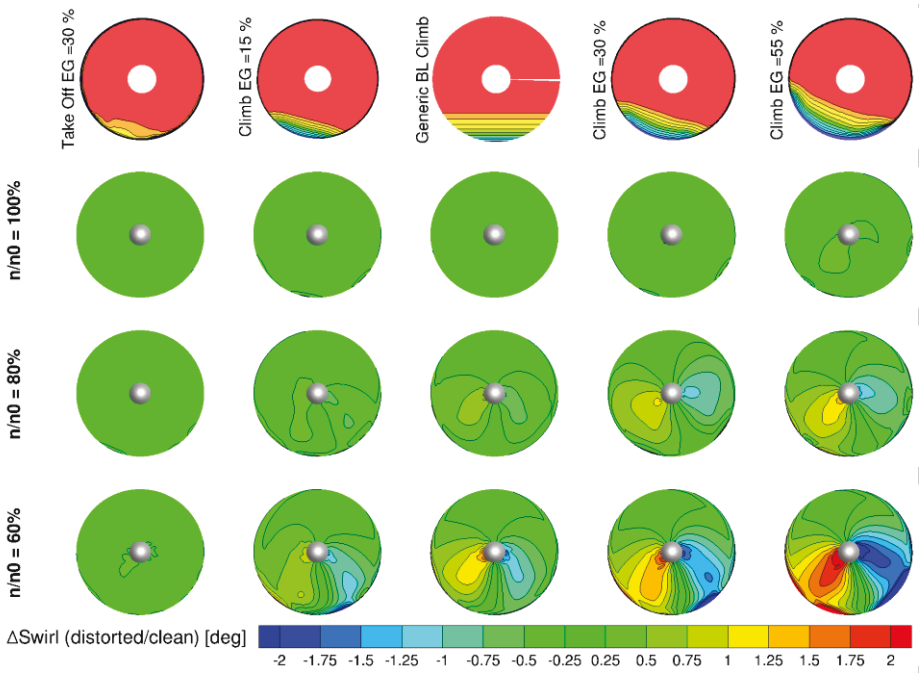

FIG 15. Tangential velocity angle difference contours upstream of the fan (E3) for several computed distortions and rotational speed

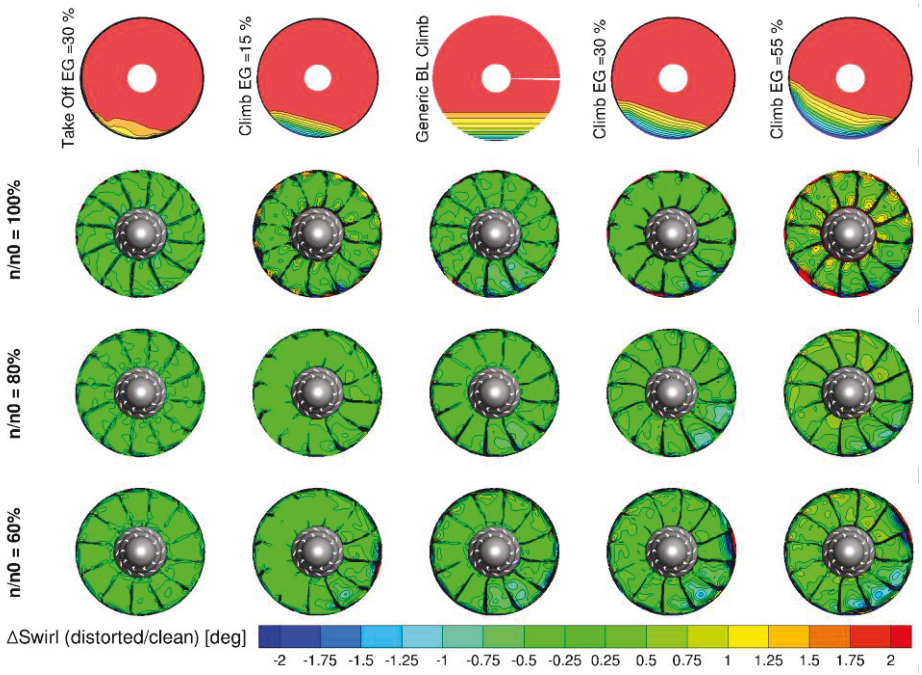

FIG 16. Tangential velocity angle difference contours downstream of the fan (E5) for several computed distortions and rotational speed.

Fig 15 presents the time-averaged tangential velocity angle difference contours at the E3 plane located upstream of the fan. Here again the distortion effects are stronger for lower rotational speed: the co-swirl and counter-swirl zones are bigger for lower RPM. In fact, as the RPM decreases, the meridional Mach number decreases also, which increases flow deflection for the same pressure gradient.

Downstream of the fan, the tangential velocity angle difference values are very small (see Fig 16); this highlights the positive effects of the fan in attenuating the distortion effects.

Fig 17 presents the static pressure difference contour at the tip region of rotor 1 and rotor 2. It is noticeable that there is, over the circumference, a difference between the passages with and without distortion. This confirm the presence of local operating points.

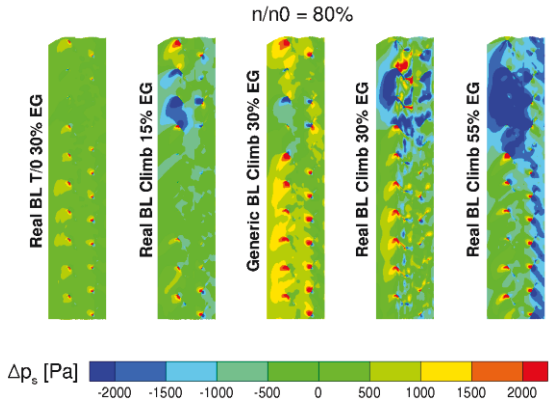

FIG 17. Static pressure difference contours at the fan tip wall (80% RPM)

4. CONCLUSION

The present study gave details about the aerodynamic effects induced by BLI/fan interactions. Several total pressure distortions, corresponding to different embedded engines and flight conditions, were considered. The results show good agreement to the observations found in the literature. The main conclusions can be drawn as follows:

- for each RPM, the distortions decrease the isentropic efficiency; this is most likely due to pressure rise difference between the distortion levels.
- for a same embedded engine, the distortion is stronger when the fan operates at cruise or climb.
- for a given total pressure distortion, the fan has lower performances for lower RPM, due to increased flow deflection and resulting swirl.
- for a given flight condition (ie climb), the deeper the engine embedded is, the stronger distortion effects are.
- a flat plate boundary layer has lower aerodynamic effects than an a/c fuselage boundary layer: the boundary layer concept is thus much beneficial for the “flat-body aircrafts” than the “conventional aircrafts”.

Although the BLI concept is quite promising for improving energy consumption, it still limits the fan's aerodynamic performances (isentropic efficiency and stability limit). A balance should therefore be found between these two aspects of the BLI.

ACKNOWLEDGMENT

The authors would like to acknowledge A. Vinz of the department “Transportflugzeuge” (AS-TFZ) of DLR for providing full aircraft CFD results. We would also like to thank M. Mennicken and D. Schoenweitz of the “Fan und Verdichter” (AT-FUV) department. for all the useful support they provided on the Harmonic Balance settings.

REFERENCES

[1] Giuliani J., Beach T., Chen J., Bakhle M.: Numerical Simulation of Boundary Layer Ingesting (BLI) Inlet/Fan Interaction, 50th AIAA/ASME/SAE/ASEE Joint Propulsion Conference, Cleveland, Ohio, July 2014.

[2] Goerke D.; Le Denmat A.-L.; Schmidt T.; Kocian F.; Nicke E.: Aerodynamic and Mechanical Optimization of CF/PEEK Blades of a Counter Rotating Fan, Proc. ASME. 44731; Volume 7: Structures and Dynamics, Parts A and B :21-33.June 11, 2012, Copenhagen Denmark GT2012-68797, doi: 10.1115/GT2012-68797, 2012.

[3] Schoenweitz, D., Schnell, R.: Development and Evaluation of a Performance Estimation Methodology for Fans Operating within non-homogeneous Inflow, ASME Turbo Expo Seoul/Korea, 2016.

[4] Hardin L. W., Tillman G., Sharma O. P., Berton J., Arend D. J..: Aircraft System Study of Boundary Layer Ingesting Propulsion, 48th AIAA/ASME/SAE/ASEE Joint Propulsion Conference, Atlanta, Georgia, July 2012.

[5] Kirner R., Raffaelli L., Rolt A., Laskaridis P., Doulgeris G., Singh R.: An assessment of distributed propulsion: Advanced propulsion system architectures for conventional aircraft configurations, Aerospace Science and Technology, June 2015.

[6] Smith, L. H.: Wake Ingestion Propulsion Benefit, Journal of Propulsion and Power, 1993, pp. 74-82.

[7] Gomar A.: Multi-Frequential Harmonic Balance Approach for the Simulation of Contra-rotating

Open Rotors : Application to Aeroelasticity, phD thesis at Arts et Métiers ParisTech – Centre de Paris CERFACS & Dynfluid, pp. 34-45.

[8] Frey C., Ashcroft G., Kersken H.-P., Schoenweitz, D., Mennicken, M.: Simulation of Indexing and Clocking with Harmonic Balance, International Journal of Turbomachinery Propulsion and Power, 2017.

[9] Longley, J. P., Greitzer E. M.: Inlet Distortion Effects in Aircraft Propulsion System Integration, in: Proceedings of Steady and Transient Performance Prediction of Gas Turbine Engines, AGARD-LS-183, 1992.

[10] Hall D. K., Greitzer E. M., Tam C. S. : Analysis of fan stage design attributes for boundary layer ingestion, ASME Turbo Expo Seoul/Korea, June 2016, GT2016-57808.

[11] Godard B. : Efficient operability assessment of a turbofan in distorted inlet conditions, Proceedings of ONERA-DLR Aerospace Symposium, Bonn/Germany, July 2018.

[12] Plas A. P., Sargeant M. A., Madani V., Crichton D., Greitzer E. M., Hynes T. P., Hall C. A. : Performance of a Boundary Layer Ingesting (BLI) Propulsion System, 45th AIAA Aerospace Sciences Meeting and Exhibit, Reno, Nevada, January 2007.

[13] Bakhle M. A., Reddy T. S. R., Herrick G. P., Shabbir A., Florea R. V.: Aeromechanics Analysis of a Boundary Layer Ingesting Fan, 48th AIAA/ASME/SAE/ASEE Joint Propulsion Conference, Atlanta, Georgia, July 2012.

[14] Daroukh M., Gourdain N., Moreau S., Boussuge J.-F., Sensiau C.: Impact of inlet distortion on fan tonal noise, Proceedings of 12th European Conference on Turbomachinery Fluid dynamics & Thermodynamics, Stockholm, Sweden, April 2017.